Molecular imaging of brain lipid environment of lymphocytes in amyotrophic lateral sclerosis using magnetic resonance imaging and SECARS microscopy

Machtoub L[1], Bataveljić D.[2], Andjus P. R.[2]

[1]*Universitätsklinik für Radiodiagnostik , Innsbruck Medical University, Innsbruck, Austria,*
[2] *Institute for Physiology and Biochemistry; Faculty of Biology; University of Belgrade, Serbia*

Corresponding to: lina.machtoub@i-med.ac.at,
Univ.Klinik für Radiodiagnostik, Innsbruck Medical University,
Anichstr.35, A-6020 Innsbruck, Austria

KEYWORDS: USPIO, ALS, Nanoparticles, Neurodegeneration, Lipids

Summary

This paper highlights some of the key technologies of using two innovative molecular imaging modalites, magnetic resonance imaging (MRI) and nonlinear optical microscopy, for imaging intravenously injected ultra small paramagnetic iron oxide nanoparticles cross linked with antibodies (CLUSPIO) in the amyotrophic lateral sclerosis (ALS) experimental model *in vivo* or *ex vivo*, respectively. Intensive efforts have been made in investigating the causes of abnormalities in lipid metabolism, monitored in some neurodegenerative disorders systems. It has been shown that an abnormal accumulation of some common lipids in motor nerve cells may play a critical role in the development of amyotrophic lateral sclerosis. The presented experiments were performed on brain specimens from the transgenic rat model expressing multiple copies of mutated (G93A) human SOD-1 gene, after CD4+ lymphocytes were magnetically labeled with i.v.i. CLUSPIO antibodies. *In vivo* MRI revealed marked signal intensity enhancements in specific pathological regions of the ALS rat brain as compared to the wild type. Surface-enhanced coherent anti-Stokes Raman scattering (SECARS) microscopy indicated cellular interactions based on lipids association to anti-CD4 CLUSPIO.

Introduction

Molecular imaging is playing an increasing role in clinical diagnoses and in the development and application of new drugs intended for various disease treatments. The specific imaging modalities, that are currently central in pre-clinical research and clinical routine are magnetic resonance imaging, ultrasound imaging, computed tomography, and recently some applications using optical imaging (Culver *et al.* 2008). In neuroimaging studies, high resolution structural images together with low resolution images using multiple imaging modalities are often required for better understanding of the pathology acquired from the same set of subjects of the brain chemistry. Different imaging methods have already shown their capability to function as a molecular imaging modality (Herholz *et al.* 2007). On the other hand, the spatial resolution of some of these approaches was shown to be relatively low with poor definition of anatomy. Recently MRI applications are becoming more and more dependent on contrast agents, with a very high relaxivity, such as nanoparticles containing a high payload of Gd complexes or iron oxide particles with a high payload of iron. The combination of MRI and contrast agents greatly enhances the possibilities to depict the vascular system, inflamed tissue as in arthritis, tumor angiogenesis, atherosclerotic plaques and the breakdown of the blood–brain barrier related to pathologies in neurodegenerative diseases. There have been many attempts to find the best imaging modality and to develop *in vivo* diagnostic techniques to detect the histopathological hallmarks of neurodegenerative diseases such as amyotrophic lateral sclerosis (ALS), Alzheimer's and Parkinson's diseases. The neuropathology of ALS is mostly confined to motor neurons in the cerebral cortex, motor nuclei of the brainstem, and anterior horns of the spinal cord. Upon the discovery of the mutated SOD1 in ALS (Rosen *et al*. 1993), many hypotheses have been proposed on how mutant SOD1 could cause neurodegeneration, including aberrant redox chemistry,

mitochondrial damage, excitotoxicity, microglial activation and inflammation, as well as SOD1 aggregation (McGeer *et al.* 2002; Stathopulos *et al.* 2003).

Recent studies have reported significantly elevated levels of ceramides, cholesterol esters and several other lipids in the spinal cords of people with ALS. To test whether these elevated levels of lipid species cause motor neuron degeneration associated with ALS, several investigations were carried on mice baring multiple copies of a mutated human gene for SOD1 (Cutler *et al.* 2002). As in humans, analysis of the spinal cords of these animals revealed increased levels of ceramides and cholesterol esters. I was unclear if these elevated levels are the result of cell death processes or are themselves directly contributing to it.

This paper is primarily devoted to the method of probing the cellular metabolic state based on lipids association to uptaken ultra small paramagnetic iron oxide particles (USPIO) cross linked to anti-CD4 antibodies (CLUSPIO) in the G93A ALS rat experimental model. SECARS microscopy is a newly developed nonlinear optical microscopic approach based on probing the surface enhanced Raman signal (SERS)-based biomarkers-/contrast agents which is shown to be promising towards becoming a medical diagnostic tool for both *ex vivo* and *in vivo* live cell imaging applications. The main goal of this study is to explore the mechanism underlying iron oxide cellular interactions in biological samples from an established neurodegenerative experimental animal model using a commercial CLUSPIO MRI contrast agent.

2 Material and Methods.

The experiments were performed on Sprague-Dawley rats expressing mutated (G93A) human SOD-1 gene and wild type (Taconic Farms, NY). Commercially available antibodies against CD4+ T cells, magnetically labelled with ultra small particles of iron oxide (MACS®, Miltenyi Biotec) - CLUSPIO were i.v. injected into rats via the tail vein (200 μL of original solution in 1 mL of physiological saline).

In vivo MR imaging with 1.5 T Avanto clinical MRI imager (Siemens) was performed on the ALS and WT animal models 24 hr after i.v. injected with – CLUSPIO. Two small surface RF coils placed laterally at each side of the animal head were used and three dimensional T2*W images were obtained using a gradient echo sequence (time of repetition 50 ms, time to echo 20 ms or 30 ms; voxel size 2.0 x 0.4 x 0.4 mm). Prolonging the echo time in the gradient echo T2* sequence augments the signal artefact generated by the magnetic particles, hence comparison of images obtained using different echo times becomes a reliable sign of USPIO presence in the tissue.

Rats were sacrificed 24 hr after MR imaging and brains were isolated and postfixed in 4% paraformaldehyde for 48h at +4^{o}C. For microscopic measurements the brain tissues samples were extracted from three animal models: wild type rat model, CLUSPIO- i.v.i. treated ALS and untreated ALS rat model. Further control experiments were performed on murine adipocytes, grown on gelatin-coated glass coverslips and exposed to 5 ng/mL of iron oxides nanoparticles (in total: 15 ng in 3 mL fresh medium), and extracted lipids from biological tissues, incubated in vitro with or without USPIO.

SECARS microscopy were performed using NIR excitation of ps (picosecond) mode-locked Nd:YVO4 and Ti:S laser (700-1000 nm) combined with tunable optical parametric oscillators (OPO) that cover the frequency range (200-3600 cm^{-1}). The beams are scanned over the sample and focused by water immersion objective lens with 1.2 numerical aperture. The images were recorded with a resolution of 5 s total acquisition time for one frame of 512 x 512 pixels. The microscope is designed for the signal to be detected in both forward and epi-direction. Microscopic Raman mapping images were recorded using an alpha 300R instrument (WITec, Ulm, Germany) equipped with a CCD detector. The integration time per pixel was 0.1 s. The samples were irradiated by a He Ne laser at 632.8 nm and focused by a 40 x 0.65 NA microscope objective lens.

The animal experiments were surveyed by the Committee for Animal Experimentation treated in accordance with the European Community Council Directive (Ref.Nr.86/609/EEC) and the NIH Guidelines, with approval of the Ethical Committee of the Faculty of Biology University of Belgrade.

3 Results and Discussion

According to recent studies on the ALS rat model, using clinical MRI, T_2-weighted hyperintensities have been observed in the brainstem, rubrospinal tract and vagus motor nuclei with prominent lateral ventricle and cerebral aqueduct enlargements, that are shown to be correlated to foci of neurodegeneration in these areas, not observed in the WT animals (Zang *et al.* 2004; Beers *et al.* 2008; Bataveljić *et al.* 2009; Andjus *et al.* 2009). Using magnetically labeled antibodies (against the CD4 receptor) MRI revealed the alleged accumulation of inflammatory cells in the vicinity of dilated ventricles in the interbrain regions (Fig.1).

In line with the results of MRI, using SECARS microscopy we observed marked intensity enhancement in specific pathological regions of the CLUSPIO treated ALS brain, particularly in the midbrain and the brainstem which is known to be infiltrated by helper T cells (Beers *et al.* 2008; Andjus *et al.* 2009). The prominent bands that show significant enhancement observed in the high frequency region were around 2845 and 2875 cm^{-1} (Fig.2) the typical bands for fatty acids dominated by valence vibrations of C-H_2 groups (Krafft *et al.* 2005). Particularly the band around 2850 cm^{-1} is assigned to CH_2 symmetric stretch, and the bands from 2700 to 3500 cm^{-1} are correlated to cholesterol ester (cholesteryl palmitate), triacylglyceride (glyceryl palmitate), phosphatidic acid, and sphingomyelin. Significant enhancements were also observed in the fingerprint region around 1660-1675 cm^{-1} (Fig.3). The region between 1000 and 1800 cm^{-1} is dominated by deformation vibration of the C-H_2 particularly 1130, 1299 and 1440, and around 1669 cm^{-1}, which is correlated to the steroid

ring of cholesterol. The resonance band observed around 1660 cm^{-1} is correlated to unsaturated fatty acids, serving as a typical band for lipids accumulated in the gray matter. In contrast, experiments performed in the same tuning range on the samples from untreated animals and brain tissues extracted from the wild- type rat have shown no significant indication of enhancement around these bands. The observed enhancements in the ALS brain can be correlated to accumulation of iron that might cause lipid peroxidation and degeneration in these regions. To investigate the metabolic effect of iron particles and the possibility of iron lipid binding activity, we performed several control experiments on adipocytes and lipids extracted from biological tissues, incubated *in vitro* with or without USPIO. An apparent signal enhancement could be found in the vibrational resonance wavelengths range around 2850 cm^{-1} from USPIO incubated lipids and from particular regions highlighting accumulation of iron oxide nanoparticles within adipocytes (Fig. 4). Similar measurements on control tissues have shown no indication of any enhancements. The signal enhancement has been further investigated on total brain tissues by Raman maps chemical imaging (Fig.5). Clear contrast enhancement is observed in tissues from CLUSPIO-treated ALS animals as indicated by the bright regions highlighting accumulation of iron oxide nanoparticles. To support the SERS activity of iron oxide nanoparticles, additional control microscopic Raman measurements have been performed on iron oxide nanoparticles dissolved in a specific heterocyclic organic compound (C_5H_5N; Pyridine). Clear intensity enhancement could be detected from iron oxide nanoparticles in Pyridine compared with the pure solution.

The previous results from MR imaging have shown to support a general phenomenon in the ALS model (Garbuzova-Davis *et al.* 2007; Beers *et al.* 2008; Zhong *et al.* 2008) by indicating observed infiltration of inflammatory cells (lymphocytes) into the brain tissue in the vicinity of the lateral ventricles as a consequence of a compromised blood brain barrier. Accordingly, several hypotheses have been advanced to explain the pathogenic mechanisms underlying ALS, including oxidative stress, overactivation of glutamate receptors, and apoptosis. Motor

neuron death induced by oxidative stress has been associated with increased production of ceramides and alternated subcellular cholesterol metabolism that lead to apoptosis (Pedersen *et al.* 1998). Changes in membrane lipid composition are known to affect the activities of many membrane-associated enzymes, endocytosis, exocytosis, membrane fusion and neurotransmitter uptake, and have been implicated in the pathophysiology of many neurodegenerative disorders. Increased oxidative stress in cultured motor neurons also leads to lipid alterations, and accumulation of lipid species. Namely, increased sphingolipid metabolism is implicated in the death of motor neurons and this involves increased formation of the membrane lipid peroxidation product 4-hydroxynonenal (Gurney *et al.* 1996). Moreover, studies in which sphingomyelinases were manipulated indicated that ceramide production can induce accumulation of cholesterol esters in another neurodegenerative disease, Alzheimer's, leading to increased production of amyloid peptide in cultured cells. Together, these studies implied that the neurodegenerative cascade in ALS involves an early increase in levels of oxidative stress (induced by genetic and/or environmental factors) causing disturbances in membrane lipid metabolism and resulting in the accumulation of ceramides and cholesterol esters. Nitric oxide also plays a crucial role in the activation of caspases and apoptosis, and recent studies demonstrated that its increased production is correlated with mitochondrial damage and lipid peroxidation (Kelley *et al.* 1999).

According to our results, and Raman assignments (Krafft *et al.* 2005), the observed strong lipid signal enhancement indicated high accumulation of lipids and iron particles in the brainstem and midbrain region of the ALS brain. Particularly, the observed surface-enhanced Raman signal around 2845 and 2875 cm^{-1} from CLUSPIO-treated animals and the results from our control experiments with iron oxide treated adipocytes and extracted lipids suggest the possibility of specific binding of lipid molecules to iron oxide particles. Such binding has already been demonstrated in pure lipid preparations of phosphatidylserine, and phosphatidic, oleic, and stearic acids, with the highest affinity at 5 to 10-fold on a molar basis with oleic

acid (Simpson and Petersa 1987). Moreover, recent studies have shown that iron deposits in ALS were found to be restricted to the precentral gyruses of gray matter (Ngai *et al*. 2007). From our results we could correlate the SECARS enhancement to the lipid-iron accumulation in the inflammatory cells or from regions with perturbed sphingolipid metabolism resulting in ceramide and cholesterol ester accumulation in the ALS brain.

4. Conclusion

We have investigated the effect on biolipids of CLUSPIO against CD4+ T cells in the ALS G93A rat model. Marked intensity enhancements have been observed in CLUSPIO treated ALS brain using SECARS microscopy. The observed enhancement has been correlated to lipid peroxidation and degeneration observed in these regions, based on selective association of lipids to up-taken USPIO, which shows high accumulation in the brainstem and midbrain region. The obtained results were compared with MR imaging, which shows marked hyperintensities with prominent lateral ventricle and cerebral aqueduct enlargements in these regions. Thus, it was assumed that the antiCD4 CLUSPIO still interact with the lipid environment of the lymphocytes giving the specific SECARS enhanced signal. The optical properties of iron oxide nanoparticles based on SERS are shown to be promising for future magnetic and optical probes for live cell imaging and investigation on neurodegenerative disorders.

Acknowledgment

Wyeth Research and ALSA are acknowledged for making the laboratory animals available through Taconic. The project was supported by the national grant 143054 MSTD RS.

.

References

ANDJUS P.R, BATAVELJIĆ D,VANHOUTTE G, MITRECIC D, PIZZOLANTE F, DJOGO N, NICAISE C, GANKAM KENGNE F, GANGITANO C, MICHETTI F, VAN DER LINDEN A, ROCHET R, BAĆIĆ G: In vivo morphological changes in animal models of amyotrophic lateral sclerosis and Alzheimer's-like disease: *MRI approach. Anatom. Rec.* **292:** 1882-1892, 2009.

BATAVELJIĆ D, DJOGO N, ŻUPUNSKI L, BAJIĆ A, NICAISE C, POCHET P, BAĆIĆ G, ANDJUS P.R: Live monitoring of brain damage in the rat model of amyotrophic lateral sclerosis. *Gen. Physiol. Biophys.* **28**: 212-218,2009.

BEERS DR, HENKEL JS, ZHAO W, WANG J,APPEL SH: CD4+ T cells support glial neuroprotection, slow disease progression, and modify glial morphology in an animal model of inherited ALS. *Proc. Natl. Acad. Sci. U. S. A.* **105:** 15558-15563,2008.

CULVER J, AKERS W, ACHILEFU S: Multimodalilty molecular imaging with combined optical SPECT/PET modalities. *J Nucl Med.* **49**: 169-172 , 2008.

CUTLER R, PEDERSEN W, CAMANDOLA S, JEFFREY D, ROTHSTEIN D, MATTSON M: Evidence that accumulation of ceramides and cholesterol esters mediates oxidative stress-induced death of motor neurons in amyotrophic lateral sclerosis. *Ann Neurol*. **52**:448-457, 2002.

DEMASI M, BECHARA E.J.H : Chlorpromazine Stimulatory Effect on Iron Uptake by Rat Brain Synaptosomes. *Biochemical Pharmacology*. **51**: 331-337,1996.

GARBUZOVA-DAVIS S, SAPORTA S, HALER E, KOLOMEY I, BERNET SP, POTTER, SANBERG PR: Evidence of compromised blood-spinal cord barrier in early and late symptomatic SOD1 mice modeling ALS.*PLoS ONE* **2:**e1205,2007.

GURNEY ME, CUTTING FB, ZHAI P DOBLE A, TYLOR CP, ANDRUS PK,HALL ED: Benefit of vitamin E, riluzole, and gabapentin in a transgenic model of familial amyotrophic lateral sclerosis. *Ann.Neurol*. **39:**147-157,1996.

HERHOLZ K, CARTER F, JONES M: Positron emission tomography imaging in dementia. *The British Journal of Radiology*. **80**: S160–S167, 2007.

KELLEY E, WAGNER B, BUETTNER G, BURNS C.P: Nitric oxide inhibits iron-induced lipid peroxidation in HL-60 cells. *Archives of Biochemistry andBiophysics.* **370**: 97-104,1999.

KE Y, HO K, DU J, ZHU L, XU Y,WANG O, WANG C, LI L, GE X, CHANG Y, QIAN Z: Role of soluble ceruloplasmin in iron uptake by midbrain and hippocampus neurons. *J Cell Biochem.* **98**: 912-919,2006.

KRAFFT C, NEUDERT L., SIMAT T, SALZER R**:** Near infrared Raman spectra of human brain lipids**.** *Spectrochim Acta Part* A **61:**1529-1535, 2005.

MCGEER PL, MCGEER EG: Inflammatory processes in amyotrophic lateral sclerosis. *Muscle Nerve* **26**:459-470, 2002.

NGAI S, TANG Y, DU L, STUCKEY S: Hyperintensity of the Precentral Gyral Subcortical White Matter and Hypointensity of the Precentral Gyrus on Fluid-Attenuated Inversion Recovery: Variation with Age and Implications for the Diagnosis of Amyotrophic Lateral Sclerosis. *J Neuroradiol*,**28**: 250-254,2007.

PEDERSEN WA, FU W, KELLER JN: Protein modification by the lipid peroxidation product 4-hydroxynonenal in the spinal cords of amyotrophic lateral sclerosis patients. *Ann Neurol.***44**:819-829,1998.

ROSEN DR, SIDDIQUE T, PATTERSON D, FIGLEWICZ DA, SAPP P, HENTATI A, DONALDSON D, GOTO J, O'REGAN JP, DENG HX, RAHMANI Z, KRIZUS A, MCKENNA-YASEK D, CAYABYAB A, GASTON SM, BERGER R, TANZI RE, HALPERIN JJ, HERZFELDT B, VAN DEN BERGH R, HUNG W-Y, BIRD T, DENG G, MULDER DW, SMYTH C, LAING NG, SORIANO E, PERICAK–VANCE MA, HAINES J, ROULEAU GA, GUSELLA JS, HORVITZ RH, BROWN JR RH: Mutations in Cu/Zn superoxide dismutase gene are associated with familial amyotrophic lateral sclerosis. *Nature* **362**:59–62, 1993.

SIMPSON R, PETERSA T: Iron-binding lipids of rabbit duodenal brush-border membrane. *Biochimica et Biophysica Acta (BBA) – Biomembranes* **898**: 181-186,1987.

STATHOPULOS P. B, RUMFELDT J. A, SCHOLZ G. A, Iani R.A, FREY H:E. HALLEWELL R:A, LEPOCK J.R, MEIERING E:M: Cu/Zn Superoxide Dismutase Mutants Associated with Amyotrophic Lateral Sclerosis Show Enhanced Formation of Aggregates in vitro. *Proc Natl Acad Sci USA* **100**, 7021-7026 , 2003.

TERRASA A.M, GUAJARDOA M. H, SANABRIA E, CATALÁ : Pulmonary surfactant protein A inhibits the lipid peroxidation stimulated by linoleic acid hydroperoxide of rat lung mitochondria and microsomes. *Biochimica et Biophysica Acta (BBA)* .**1735**: 101-110, 2005.

ZANG DW, YANG Q, WANG HX, EGAN G, LOPES EC, CHEEMA SS: Magnetic resonance imaging reveals neuronal degeneration in the brainstem of the superoxide dismutase 1 transgenic mouse model of amyotrophic lateral sclerosis. *Eur J Neurosci* **20**: 1745–1751, 2004.

ZHONG Z, DEANE R, ALI Z, PARISI M, SHAPOVALOV Y, O'BANION MK, STOJANOVIC K, SAGARE A, BOILLEE S, CLEVELAND DW, ZLOKOVIC BV: ALS-causing SOD1 mutants generate vascular changes prior to motor neuron degeneration. *Nat Neurosci* **11**: 420–422, 2008.

Figures captions

Figure 1. MRI of the brain of the ALS rat treated with CLUSPIO ("ALS-CLU") as compared to the MRI of the ALS rat without CLUSPIO injection ("ALS") and of the wild type rat ("WT"). T2W protocol reveals the dilated ventricles in the ALS model (images in the left column). T2* protocol reveals the hypointensities (note regions delimited by ellipsoids)

allegedly caused by CLUSPIO seen with time to echo (TE) 25 ms (middle column) and further augmented with TE 35 ms (right column).

Figure 2. SECARS image of brain tissue from CLUSPIO treated ALS rats, taken at (A) 2875 cm^{-1} and (B) at 2850 cm^{-1}. (C) The corresponding cross section profile shows intensity enhancement along the indicated line shown in the inset of the SECARS image

Figure 3. SECARS image of brain tissue from CLUSPIO- treated ALS rats taken in the finger print region around 1660 cm^{-1}

Figure 4. (A) SECARS image of adipocytes treated with iron oxide nanoparticles (bright regions), taken around 2850 cm^{-1}. (B) Gray scale plot shows the intensity enhancement highlighting the accumulation of iron oxides nanoparticles indicated by arrow (inset).

Figure 5. Raman spectrum extracted from the Raman map image (inset, scale bar 1 µm) of brain tissue from CLUSPIO treated ALS rats, in the range of 200-3100cm^{-1}.

Figure 1

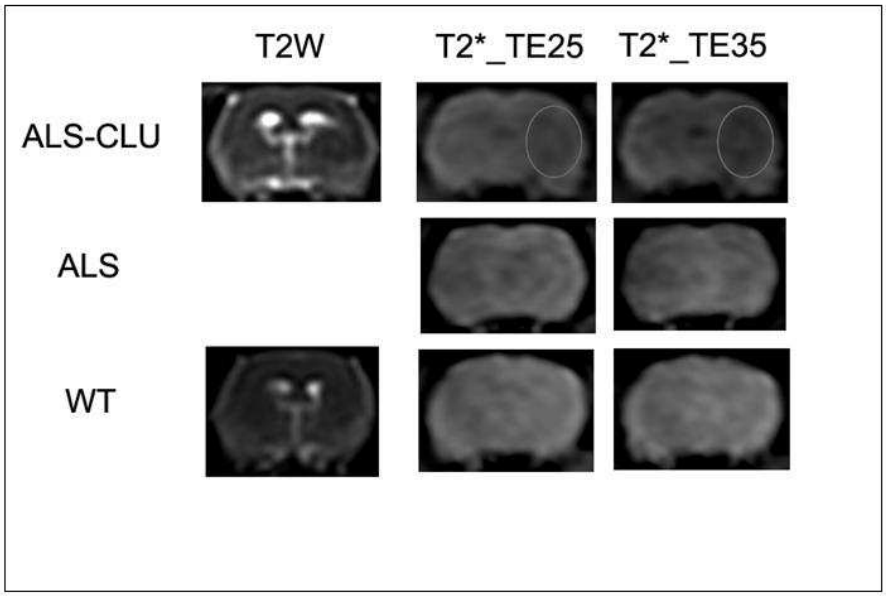

Figure 2

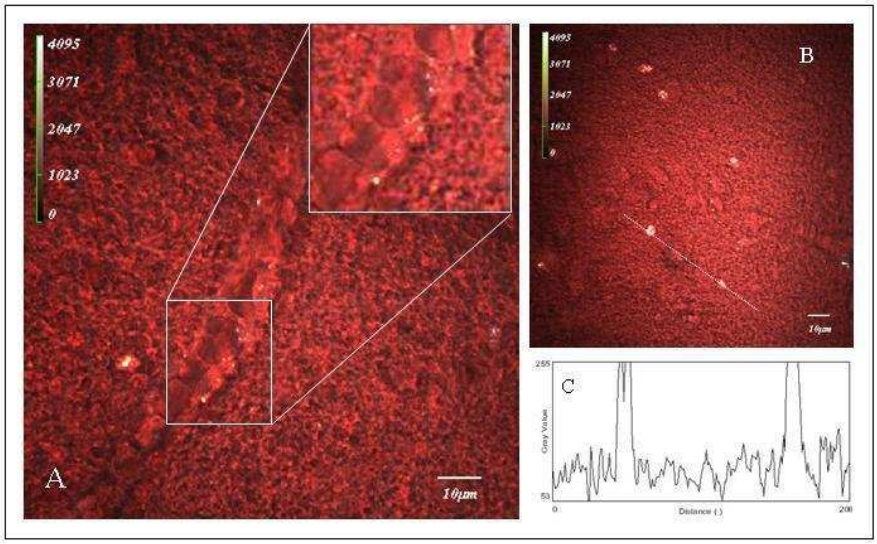

Figure 3

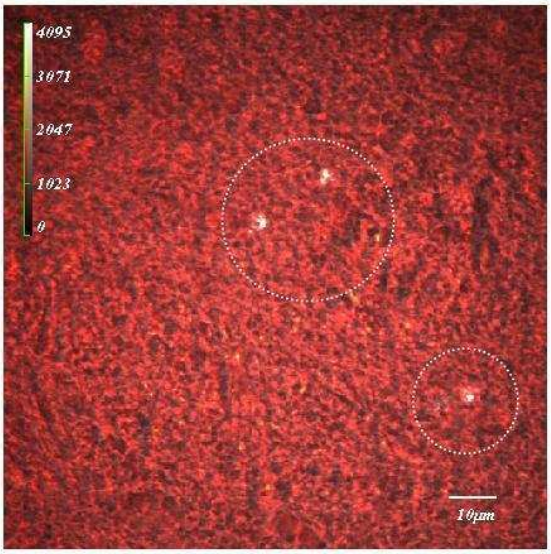

Figure 4

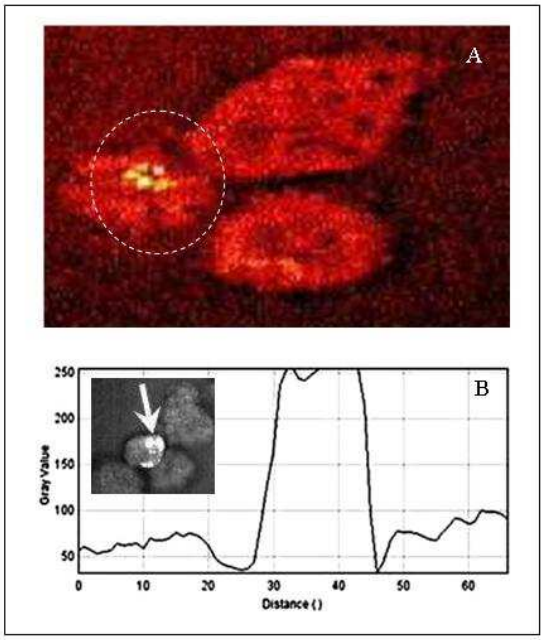

Figure 5

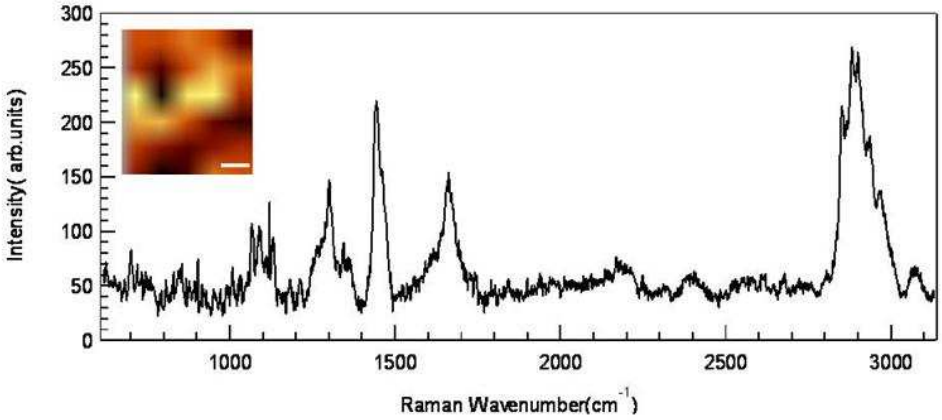
Intensity(arb.units)
300
250
200
150
100
50
0
1000
1500
2000
2500
3000
Raman Wavenumber(cm-1)